NASA TM X-62,262

NASA TECHNICAL MEMORANDUM

NASA TM X-62,262

OBSERVATIONS OF DISK-SHAPED BODIES IN FREE FLIGHT AT TERMINAL VELOCITY

John W. Vorreiter and David L. Tate

Ames Research Center
Moffett Field, Calif. 94035
and
Kirtland Air Force Base
New Mexico 87117

March 1973

OBSERVATIONS OF DISK-SHAPED BODIES IN FREE FLIGHT AT TERMINAL VELOCITY

by

John W. Vorreiter*
NASA-Ames Research Center
Moffett Field, California 94035

and

David L. Tate**
Kirtland Air Force Base, New Mexico

*Research Scientist
**Lt., USAF

SUMMARY

Ten disk-shaped models of a proposed nuclear heat source module were released from an aircraft and observed by radar. The initial launch attitude, spin rate and mass of the models was varied. Significant differences were observed in the mode of flight and terminal velocity among models of different mass and among models with different launch attitudes. The data were analyzed to yield lift and drag coefficients as a function of Reynolds number. The total sea-level velocity of the models was found to be well correlated as a function of mass per unit frontal area. The demonstrated terminal velocity of the modular disk heat source, about 27m/sec for this specific design, is only 33 percent of that of existing heat source designs.

INTRODUCTION

The purpose of this investigation was to determine the subsonic free-flight behavior of disk-shaped bodies having ballistic coefficients of the order of 60 kg/m^2. Such bodies are of interest as containment systems for radioactive materials destined for space. If released as a result of a flight abort during launch or orbital insertion maneuvers they can be shown to suffer a milder reentry than several contemporary designs, and to impact the ground at lower terminal velocities.

A candidate shape that most conveniently meets the requirement of high drag to mass ratio and is also compatible with normal operation in space nuclear power systems is a flat disk. The behavior of these objects (disk modules) in subsonic free flight has not been investigated and was the purpose of this test.

Related work by Bustamante (Ref.'s 1, 2 and 3) on rectangular plates, by Smith (Ref. 4) on rectangular wings, and by Willmarth (Ref. 5) on free-falling disks in liquids suggests at least 3 different flight modes. These are:

1. stable flat down.
2. flat down oscillating with large side-to-side excursions.
3. autorotating, which is continuous tumble at constant rate.

For the range of expected velocities, or more important, the range of expected Reynolds numbers, the stable and oscillating modes were expected to be transitory modes and the disks of interest were expected to eventually come to a state of dynamic equilibrium in the autorotating mode.

SYMBOLS

A	frontal area	(m^2)
C_D	Drag coefficient	
C_L	Lift coefficient	
D	Body diameter	(m)
g	gravitational constant	(m/sec^2)
m	Mass (kg)	
R_N	Reynolds number	
V_H	Velocity in horizontal direction	(m/s)
V_T	Total velocity	(m/s)
V_X	Velocity in X direction	(m/s)
V_Y	Velocity in Y direction	(m/s)
V_Z	Velocity in Z direction	(m/s)
γ	flight path angle as measured from the horizontal	(deg)
μ	local air viscosity (kg/m-sec)	
ρ	local atmospheric density	(kg/m^3)
ω	rotational rate	(radians/sec)

EQUIPMENT AND PROCEDURES

Ten disk modules of three masses were constructed as shown in Figure 1. All were 18.28cm in diameter with .46cm radius edges. Six disk modules (Type A) had a mass of 1.64Kg, a polar moment of inertia of 7.04×10^{-6} Kg-m^2 and a moment of inertia in the plane perpendicular to the polar axis of 3.16×10^{-6} Kg-m^2. A tentative design for a 240-watt modular radioisotope disk module heat source is within 1-2 percent of all three of these properties. To provide information for other weights and moments that would cover any possible design changes, these same physical quantities were doubled for Type B disk modules and halved for Type C. The Type B disk module was almost completely composed of lead.

The disk modules were dropped one at a time on June 20, 1972, from the rear of a C-130 aircraft flying at about 4600m altitude (above sea level) over the White Sands Missile Range. They were then skin-tracked by Radar Station #R-128 which is equipped with an AN/FPS-16 radar set. No photographic coverage was available. Figure 2 shows the test setup and coordinate system. A balloon sounding was made from a site approximately 15 miles distant from the drop zone. This ascension began almost simultaneously with the first drop and was used to measure local wind velocity, wind direction, and air density. These wind data expressed as x and y components are shown in Figure 3.

The disk modules were given different initial attitudes and spin rates as they were thrown by hand from the aircraft. These initial conditions were either (1) random, (2) horizontal spin stabilized or (3) vertical spin stabilized. These initial launch conditions are defined as follows:

"Random Orientation, Low Spin and Tumble" means that the body was hand-launched with as small a tumble and spin rate as was achievable. The initial orientation of the body was considered to be unimportant.

"Horizontal Spin Stabilized" means the disk flats were initially horizontal and the disk was spinning about its polar axis. The method of release from the aircraft was like the hurl of a discus. Tests show that spin rates of from 5 to 10 rev/sec probably were obtainable by this means.

"Vertical Spin Stabilized" is identical to horizontal spin stabilized except that the disk flats were initially vertical.

Table 1 identifies which models were released in the various initial attitudes.

RESULTS AND DISCUSSION

The data were supplied to us by the White Sands Missile Range personnel in the form of position (x, y, and z coordinates) and corresponding velocity and acceleration components for time increments of 0.1 second. Data were available from near the point of release to about 1500m altitude where the objects were lost in the radar ground return. Because of the large horizontal component of velocity imparted to the disks at the point of release by the aircraft and the ground clutter problem at low altitude, only the data from altitudes of 3600m to 1800m were used. The component velocities were vectorially added to yield a total velocity. This total velocity, along with each of the components, is shown in Figure 4 for Model A1.

The x component (V_X), the y component (V_Y), and total velocity (V_T) (Fig. 4) show large sine-like variations with altitude. The sources of these oscillations is much better understood when the measured x and y components of the wind vector are subtracted from the observed x and y velocity components of the body. The data so modified are shown in Figure 5. From this figure it is clearly evident that the x and y velocity components change in a sine-cosine manner and the z component shows a slow change with atmospheric density. Such a sine-cosine variation can be generated by a body falling in a spiral or helical path. Even with the wind effect taken into account the z component of velocity shows low-amplitude sinusoidal variations with altitude which are thought to be due to an imperfect accounting for the effect of the wind.

The wind-corrected data for models A2 through C2 are shown in Figures 6 through 14. All the data appear to be of high quality with two exceptions. These exceptions are the data for Model A5 below an altitude of about 2000m and the data for Model C1 at about 2100m altitude. These data appear erratic, are thought to be in error or the result of local wind gusts, and therefore, were not used.

The lift and drag coefficients for each body were determined from the velocity component data. A sketch of the forces acting

on a body is shown in Figure 15. Since all accelerations are very small, a component force balance can be made in the x and z directions as follows:

$\Sigma F_x = 0$

$$(\text{Lift}) \times [\cos (90° - \gamma)] = (\text{Drag}) \times (\cos \gamma)$$

since: $\text{Lift} = 1/2\ \rho\ V_T^2\ C_L A$

$\text{Drag} = 1/2\ \rho\ V_T^2\ C_D A$

$\text{Cos}\ (90° - \gamma) = \text{Sin}\ \gamma$

$$1/2\ \rho\ V_T^2\ C_L A\ \text{Sin}\ \gamma = 1/2\ \rho\ V_T^2\ C_D A \cos \gamma$$

or

$$\frac{\text{Sin}\ \gamma}{\cos \gamma} = \tan \gamma = C_D/C_L \qquad (1)$$

$\Sigma F_z = 0$

$$(\text{Lift})[\sin (90° - \gamma)] + \text{Drag}\ (\sin \gamma) = mg$$

or

$$C_L \cos \gamma + C_D \sin \gamma = \frac{2mg}{\rho\ V_T^2\ A} \qquad (2)$$

The velocity components can be resolved to horizontal and vertical velocities as shown in Figure 16. This transformation yields a third equation, namely;

$$\tan \gamma = \frac{V_z}{V_H} \qquad (3)$$

Therefore, three equations are available to solve for the three unknowns, C_L, C_D, and γ. These equations simplify to:

$$C_D = \frac{2mg}{\left[\left(\frac{V_H \cos\gamma}{V_z}\right) + \sin \gamma\right] \rho\ V_T^2\ A} \qquad (4)$$

and

$$C_L = C_D / \tan \gamma \qquad (5)$$

Equations 3, 4, and 5 can then be solved for each individual radar observation; A sampling of the values of C_L and C_D for all models is shown in Figure 17, as a function of Reynolds number where Reynolds number (R_N) is defined as:

$$R_N = \frac{V_T D \rho}{\mu} \qquad (6)$$

For bodies of all three masses, a noticeable decrease in drag coefficient was observed with increasing Reynolds number. However, each body of separate mass exhibited its own unique function of lift coefficient vs Reynolds number. Only the data from the type B models (3.36 kg) shows a decrease in lift coefficient vs Reynolds number. Type A and C models demonstrated a somewhat erratic variation with no clear data trend evident.

A statistical examination of the lift and drag coefficient data was made in an attempt to discover whether or not differences between the various initial launching attitudes influenced the behavior of the bodies at terminal velocity. About 250 individual data sets were analyzed for each body. These results are presented along with their standard deviations in Table 2.

The lift coefficient was found to vary from 0.176 to 0.601 for the different models with the mean value being 0.344. The Type A models launched with a horizontal spin had a 66 percent lower lift coefficient than those launched with a vertical spin. The reason for these differences is not known.

The drag coefficient was found to vary from a minimum of 1.002 to a maximum of 1.364 with a mean value of 1.184. As with the lift data, the lowest values were for the horizontally stabilized Type A models and the highest were for the lightweight Type C models. The lift to drag ratio varied in the same manner from 0.175 to 0.441 with a mean value of 0.285.

An examination of the velocity vs altitude data shows that as the models reached lower and lower altitudes the fluctuations in total velocity became larger and larger. It is thought that this was the result of rapidly changing local wind conditions near the ground. For this reason the measured total velocity at the 1800 meter altitude point was not extrapolated to sea-level density to

determine the terminal velocity at sea-level. Instead, the statistically determined mean drag and lift coefficients were used to calculate the total sea-level velocity that is shown on Table 2. Using the mean drag coefficients, effective ballistic coefficients of 53.19 kg/m^2, 108.7 kg/m^2, and 26.11 kg/m^2 are calculated for the Type A, Type B, and Type C models, respectively.

As can be seen from Table 2, the equivalent sea-level velocities range from 26.7 m/sec to 31.36 m/sec for the 1.64 Kg models (Type A), 40.86 m/sec to 42.11 m/sec for the 3.27 Kg models (Type B) and from 18.12 m/sec to 19.06 m/sec for the lighter 0.82 Kg (Type C) models. The equivalent sea-level velocity is shown as a function of mass per unit frontal area in Figure 18. An empirical equation best representing the data for the randomly launched models is:

$$V_{T_{(\text{sea-level})}} = 5.53 + 0.467 \left(\frac{m}{A}\right) - 0.00145 \left(\frac{m}{A}\right)^2 \qquad (7)$$

restricted to:

$$30 \leq \left(\frac{m}{A}\right) \leq 130 \ \frac{kg}{m^2}$$

Although neither visual nor photographic observations were made of the objects after they were lost from view of the aircraft, it is strongly felt that all of the models autorotated during the terminal portions of flight. The reason for this belief is that the considerable amount of lift deduced from the radar data can best be accounted for by postulating an autorotating body. The spiraling flight observed for all but two of the randomly launched models is thought to be caused by gyroscopic precession. Although all elements of the models were bodies of revolution, some misalignment was thought to have occurred during assembly or because of uneven paint application. This resulted in the center of gravity being slightly displaced from the volume centroid as shown on Figure 19. When the disk autorotated, it would be expected to do so about the axis of minimum inertia thus placing the center of gravity on the axis of rotation as is also shown on Figure 19. The vectorial sum of the lift and drag forces yields a net force acting in an upward direction through the volume centroid or perhaps slightly forward of the centroid in the direction of flight. Thus, a net torque of magnitude mg x d operates on the body. This small torque on the rotating system is sufficient to cause the disk to precess or turn in the direction opposite to the direction of the

c.g. offset. However, two of the randomly launched models did not fly in a spiral pattern. These models, B1 and B2, were made almost entirely of lead and it is thought that the c.g. offsets were small enough not to cause any observable precession.

For the disks which were launched spinning, apparently the viscous damping was small enough that each disk continued to spin about its polar axis throughout the flight. When this happens, the c.g. offset rotates about the volume centroid, thus causing the precessing torque periodically to act in opposite directions. Therefore, no net precessional torque should appear, and the disk would appear not to spiral in flight. All models launched spinning, namely, A3, A4, A5, and A6 behaved in this manner.

Since the models were not photographed during their fall, the autorotation rate could not be measured. However, it is shown that in Ref. 1 the "tip speed velocity ratio" of an autorotating disk is given by the equation:

$$\frac{\omega D}{2V_T} = 0.433 \qquad (8)$$

Therefore, the 1.64 Kg models would have an autorotation rate of from 22 to 26 rev/sec.

The terminal sea level velocities of existing radioisotope heat source systems such as the Transit (Ref. 6), the SNAP 27 (Ref. 7), and the SNAP-19 Pioneer (Ref. 8), are listed below along with that measured for a Disk Modular Heat Source.

Heat Source	S.L. Terminal Velocity m/Sec
Transit	90.6 (a)
SNAP-27	86.9 (b)
SNAP-19,Pioneer	93.2 (a)
Disk Module (1.64 Kg)	29.1 (a)

(a) measured
(b) calculated

From the list it is clearly evident that the demonstrated terminal velocity of the 1.64 Kg Disk Modular Heat Source is from 31 to 33 percent that of existing systems. Although a detailed analysis of the consequences of this greatly reduced terminal velocity are not a subject of this report, it should be clear to the reader that the potential for ground-impact damage is drastically reduced with a 68 percent lower impact velocity.

Conclusions

Ten full size models of a proposed nuclear heat source module were released from an aircraft and observed by radar from 4600m altitude to about 1800m altitude. The models were all 18.29 cm diameter disks, 2.08cm thick with 0.457cm corner radius. Six of the models weighed nominally 1.64 kg. Two weighed 3.36 kg and two 0.81 kg. The initial launch attitude of the 1.64 kg models was varied. They were launched either randomly with low spin rates, horizontally stabilized (flat down) with as high a spin rate as could be achieved by hand, or vertically stabilized (edge down) again with as high a spin rate as could be achieved by hand. The first major objective of the study was to determine the sea-level terminal velocities of these bodies. The total sea-level velocity of the models was found to be fairly well correlated as a function of mass per unit frontal area.

It was found that the models launched edge down showed about a 7 percent lower equivalent sea-level terminal velocity than the randomly launched models. The horizontally spin stabilized models exhibited about a 6 percent higher equivalent sea-level velocity than the randomly launched models.

The data were analyzed to yield lift and drag coefficients as a function of Reynolds number. A slight decrease of the drag coefficient with Reynolds number was observed while the lift coefficient did not demonstrate any clear trend.

All but two of the randomly launched models were observed to fly in a helical path. This was probably caused by gyroscopic precession of a rotating body having a slight displacement of its center of gravity.

Although not observed directly, it is strongly felt that all models autorotated during flight. This is evidenced by both the considerable amount of lift observed and the observed helical flight paths of the randomly launched models. The rate of autorotation was calculated from measurements of Reference 1 to be from 22 to 26 rev/sec for the 1.64 kg models.

The demonstrated sea-level terminal velocity of the 1.64 kg modular disk heat source, about 27 m/sec, is only from 31 percent to 33 percent that of existing heat source designs.

References

1. Bustamante, A. C., and Stone, G. W., Jr.: Autorotational Characteristics of Flat Plates and Right Circular Cylinders at Subsonic Speeds. Sandia Laboratories, SC-RR-67-778, November 1967.

2. Bustamante, A. C.: Free-Fall Rotation and Aerodynamic Motion of Rectangular Plates. Sandia Laboratories, SC-RR-68-132, August 1968.

3. Bustamante, A. C., and Stone, G. W., Jr.: The Dynamic Characteristics of Autorotating Configurations in Subsonic and Hypersonic Flows. Sandia Laboratories, SC-DC-68-2395, November 1968.

4. Smith, E. H.: Autorotating Wings: An Experimental Investigation. J. Fluid Mech., 1971.

5. Willmarth, William W., Hawk, Norman E., and Harvey, Robert L.: Steady and Unsteady Motions and Wakes of Freely Falling Disks. The Physics of Fluids, February 1964.

6. Transit RTG Final Safety Analysis Report. TRW Systems, Group. TRW(A)-11464-0491, March 1971.

7. SNAP-27 Safety Report. General Electric Missiles and Space Division. DIN:6300-300, July 24, 1968.

8. SNAP-19, Pioneer F Safety Analysis Report. Teledyne Isotopes, INSD-2873-42-2, June 1971

TABLE 1

Initial Conditions → / Body Mass and Moment ↓	Random Orientation Low Spin and Tumble	Horizontal-Spin-Stabilized	Vertical-Spin-Stabilized
Body A	Model A1 Model A2	Model A3 Model A4	Model A5 Model A6
Body C (1/2 mass and Moment)	Model C1 Model C2		
Body B (Twice Mass and Moment)	Model B1 Model B2		

TABLE 2

SUMMARY, PERFORMANCE OF INDIVIDUAL MODELS

MEASUREMENTS	MODELS									
	A1	A2	A3	A4	A5	A6	B1	B2	C1	C2
Mass (Kg)	1.640	1.636	1.645	1.645	1.636	1.636	3.359	3.359	0.805	0.805
Initial Conditions	Random Low Spin	Random Low Spin	Horizontal Spin Stabilized	Horizontal Spin Stabilized	Vertical Spin Stabilized	Vertical Spin Stabilized	Random Low Spin	Random Low Spin	Random Low Spin	Random Low Spin
Equivalent Sea-level Velocity m/Sec	29.134	28.892	31.360	30.189	26.70	28.35	40.861	42.111	18.12	19.06
Mean Lift Coefficient	0.305	0.309	0.176	0.263	0.408	0.321	0.317	0.298	0.601	0.450
St. Dev. Lift Coef.	0.078	0.072	0.026	0.067	0.10	0.06	0.08	0.05	4.96	0.155
Mean Drag Coef.	1.135	1.153	1.002	1.065	1.332	1.196	1.182	1.113	1.364	1.293
St. Dev. Drag Coefficient	0.047	0.042	0.034	0.042	0.092	0.064	0.124	0.074	3.97	0.172
Number of Points Used in Analysis	266	263	252	254	254	271	188	184	255	247
C_L/C_D	.268	.264	.175	.246	.306	.268	.268	.267	.441	.348

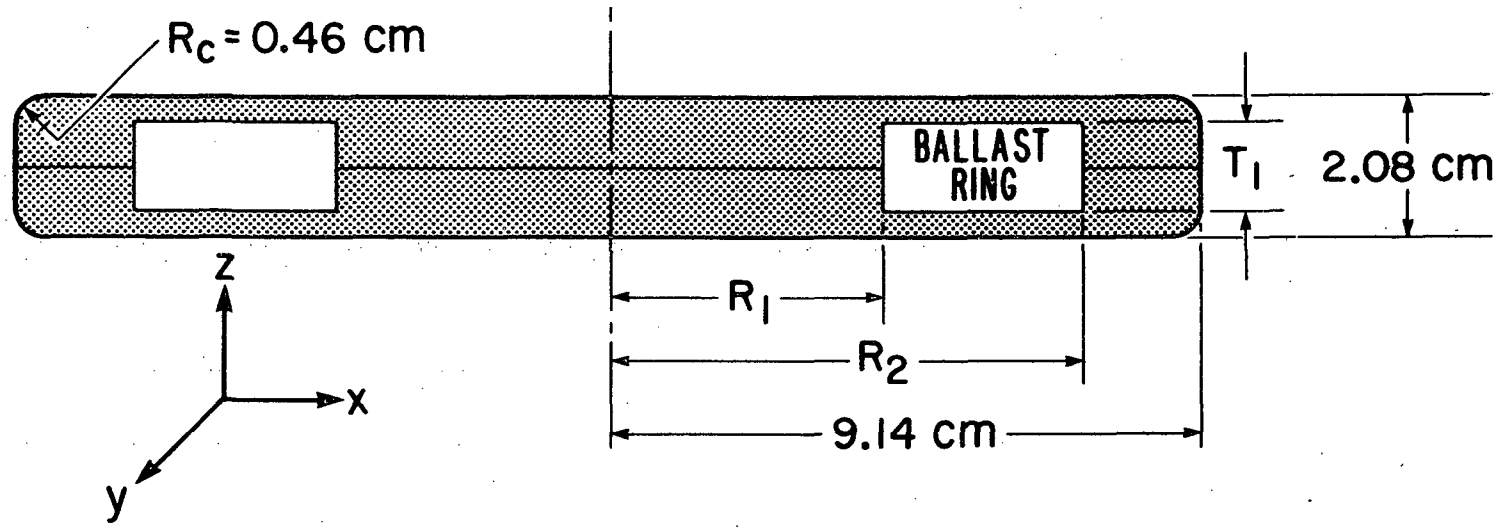

MODEL TYPE	MASS, kg	MOMENT I_z, kg-m^2, $\times 10^{-6}$	MOMENT $I_x = I_y$, kg-m^2, $\times 10^{-6}$	BALLAST MATERIAL	BASE MATERIAL	R1, cm	R2, cm	T1, cm
A	1.64	7.04	3.16	STEEL	PLEXIGLASS	4.26	7.366	1.34
B	3.36	14.09	6.34	LEAD	PLEXIGLASS	4.06	7.770	1.91
C	0.81	3.52	1.57	STEEL	PLEXIGLASS	4.09	5.067	0.94

FIGURE 1: MODEL CONFIGURATION

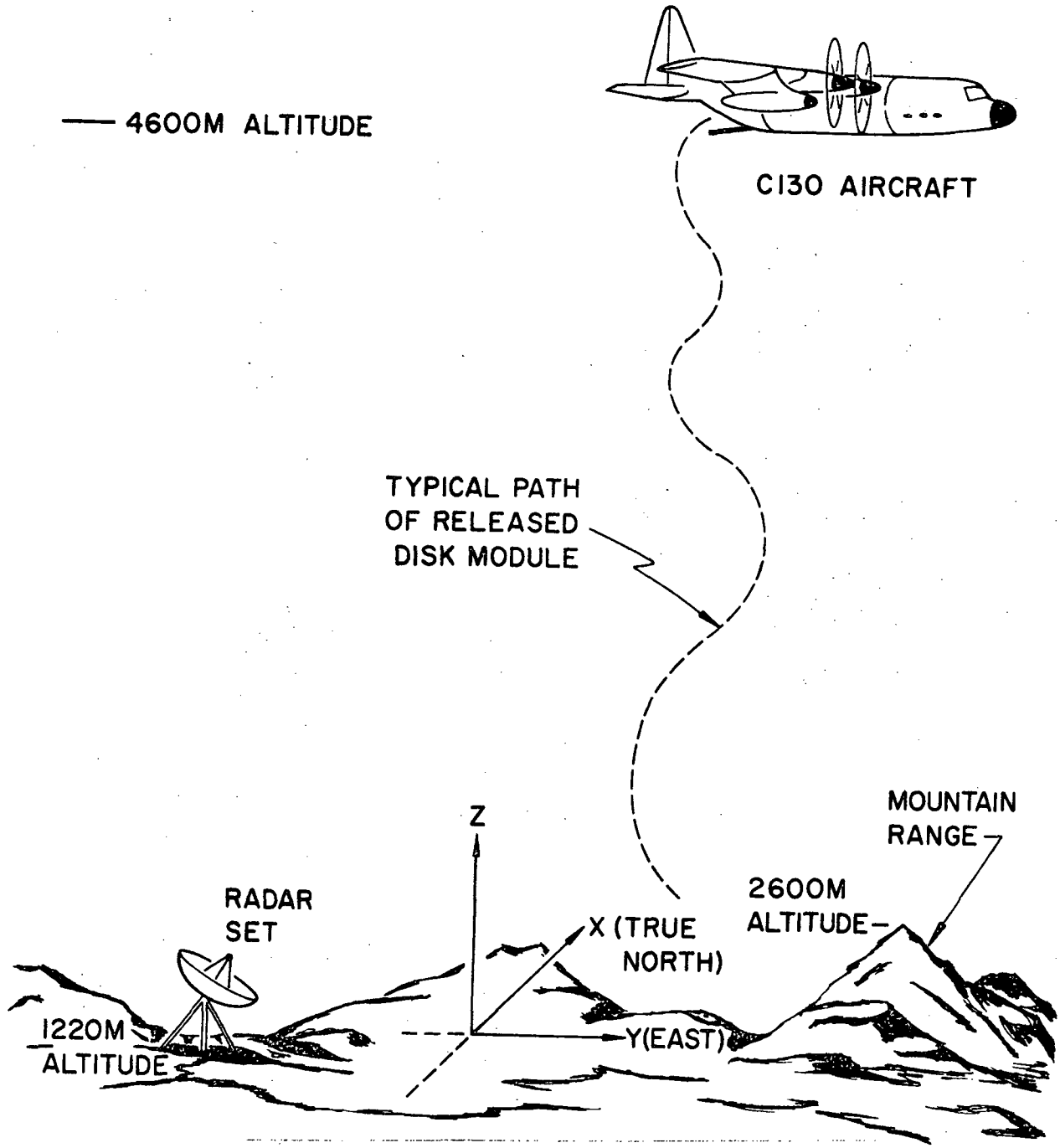

FIGURE 2: TEST SETUP AND COORDINATE SYSTEM

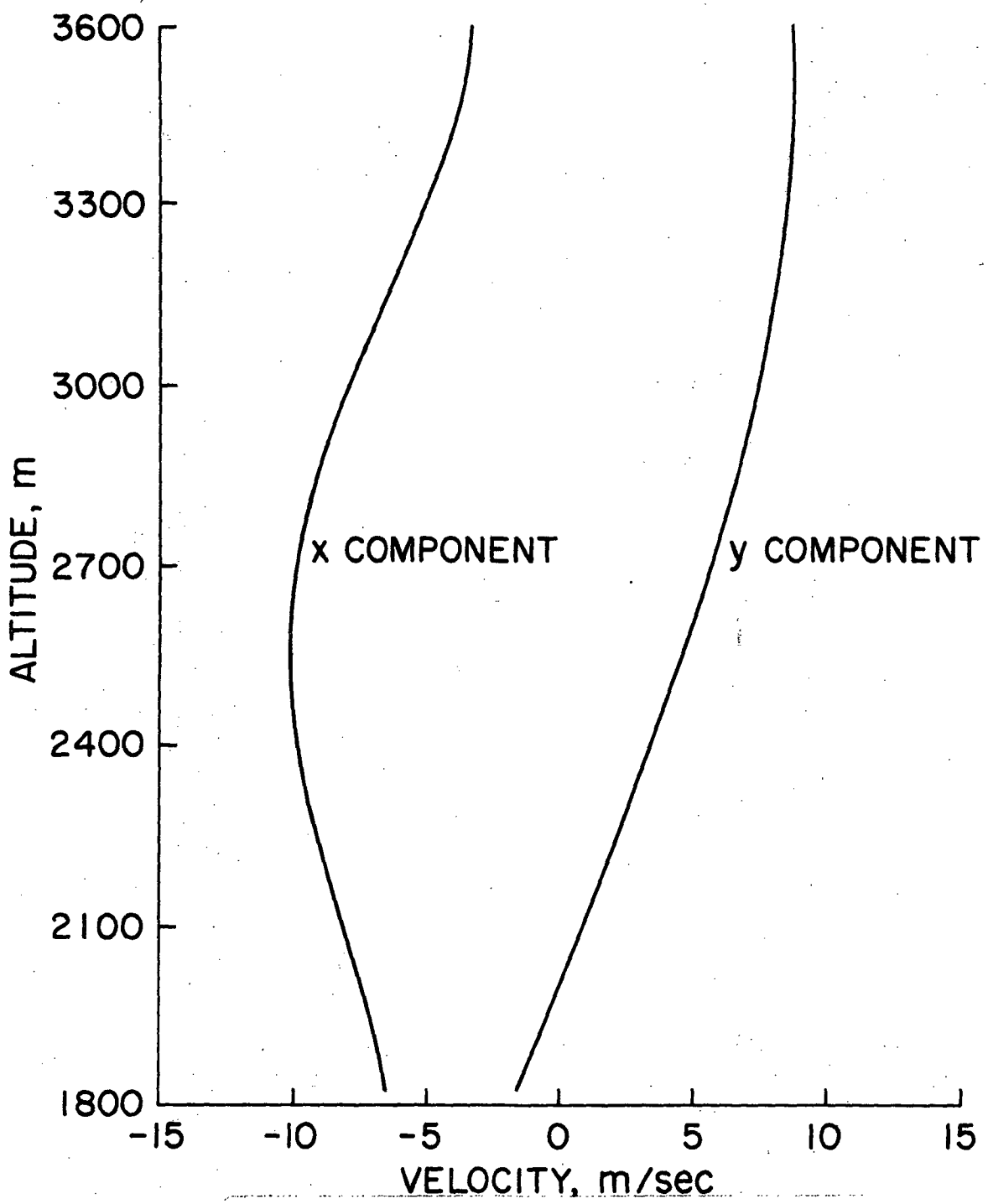

FIGURE 3:

X AND Y COMPONENTS OF WIND VELOCITY, WSMR, STALLION SITE, JUNE 20, 0845 HRS

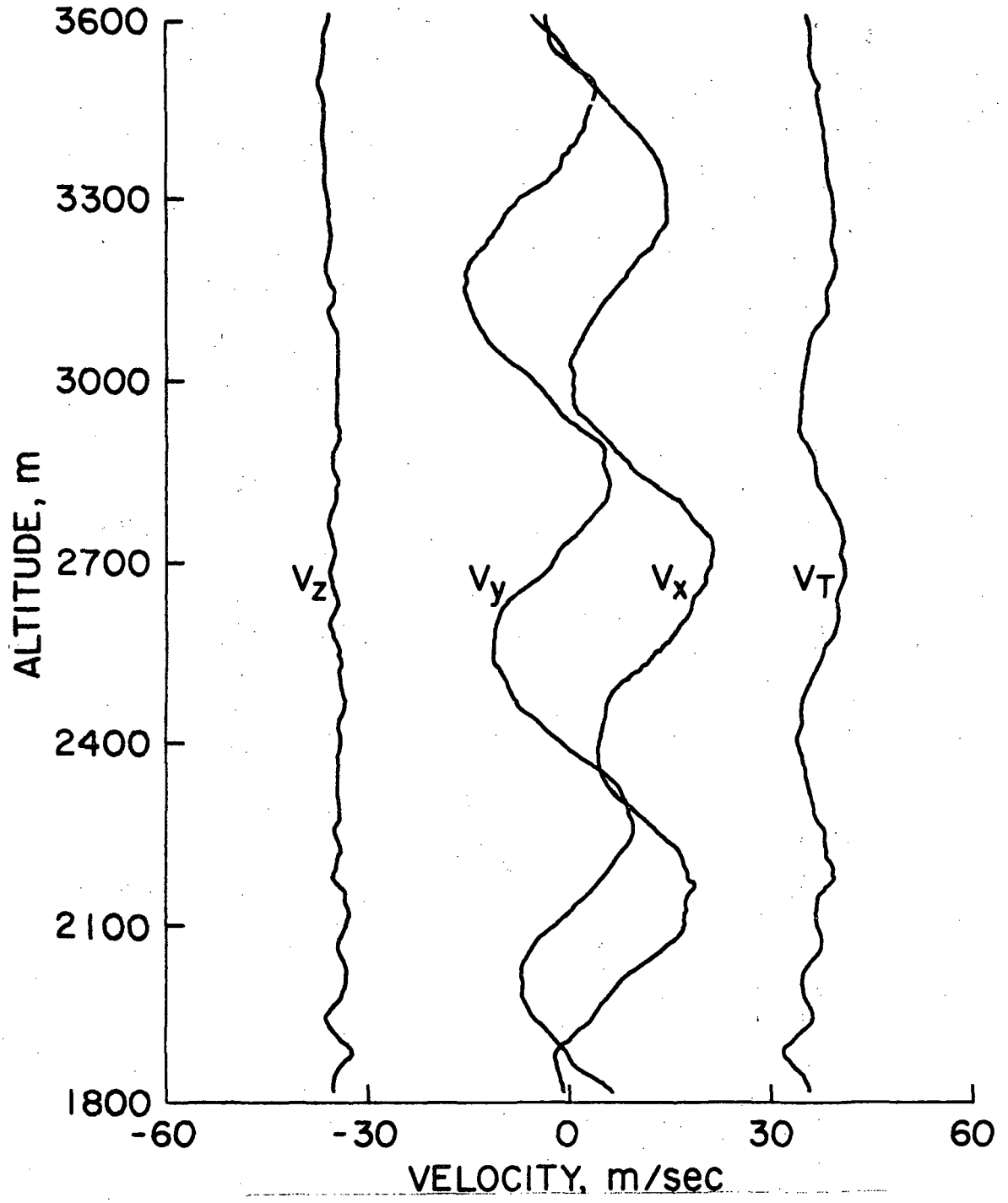

FIGURE 4:

MODEL A1, RANDOM LAUNCHED-NO WIND CORRECTION

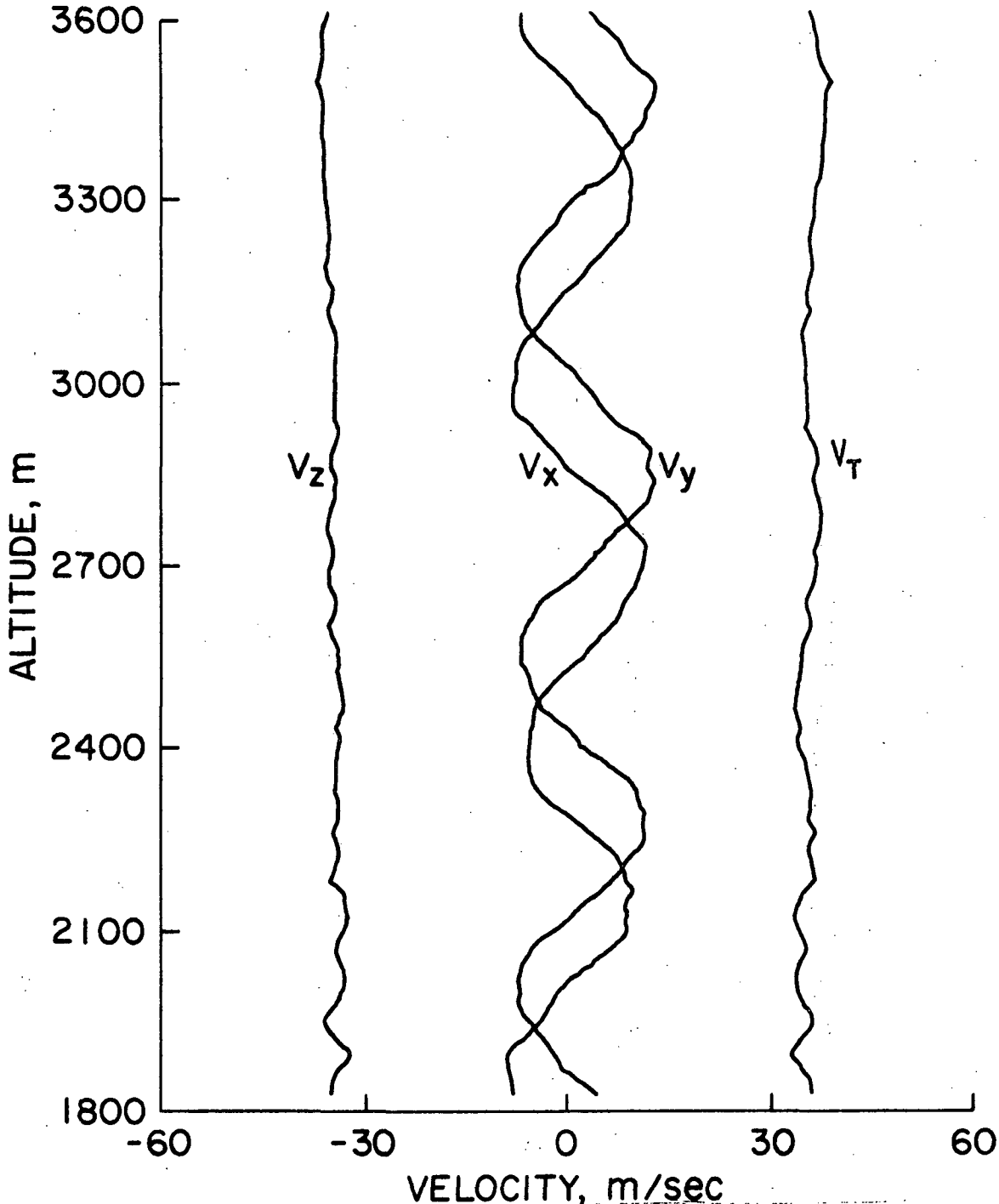

FIGURE 5:
MODEL A1, RANDOM LAUNCHED
WITH WIND CORRECTION

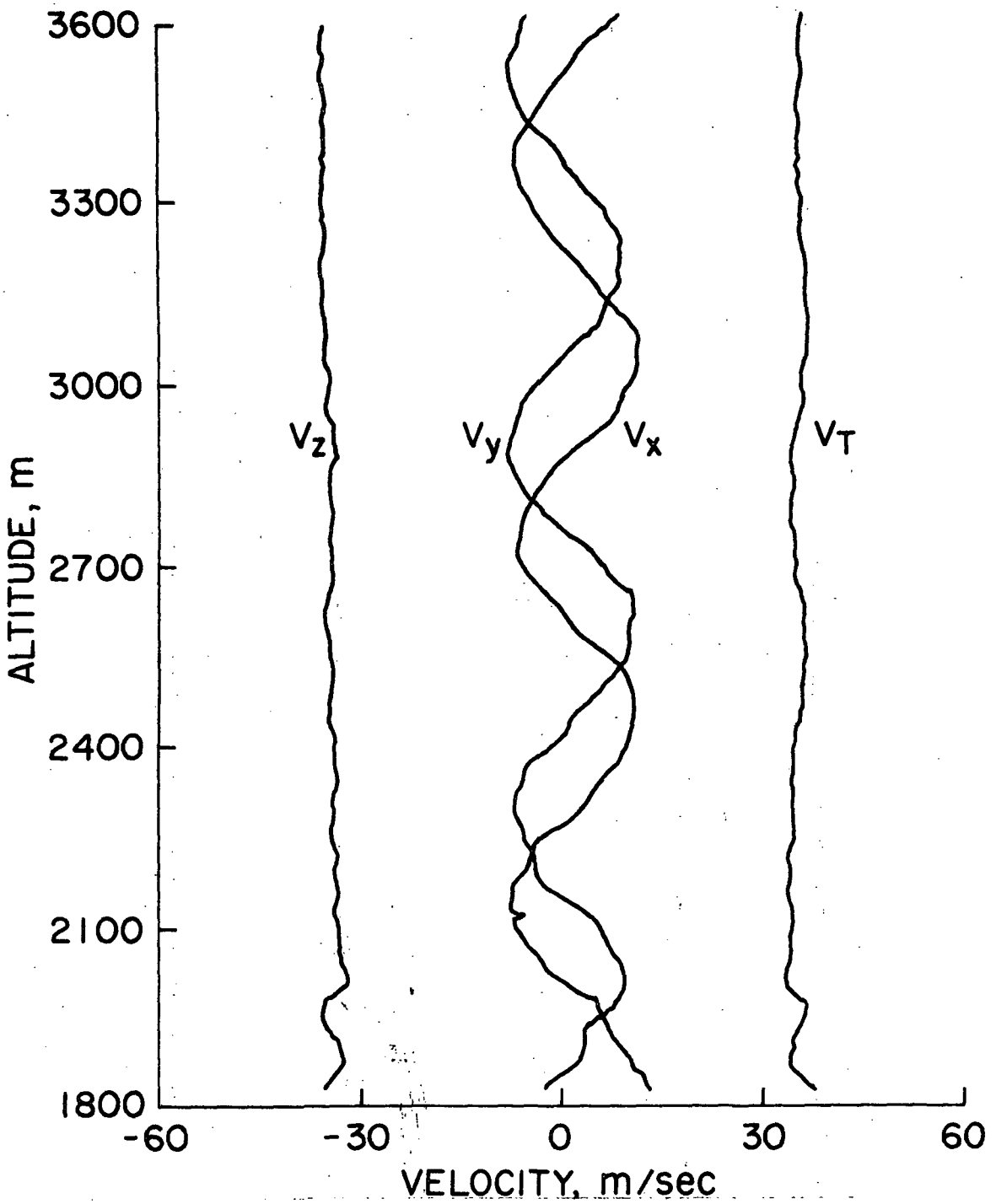

FIGURE 6:
MODEL A2, RANDOM LAUNCHED
WITH WIND CORRECTION

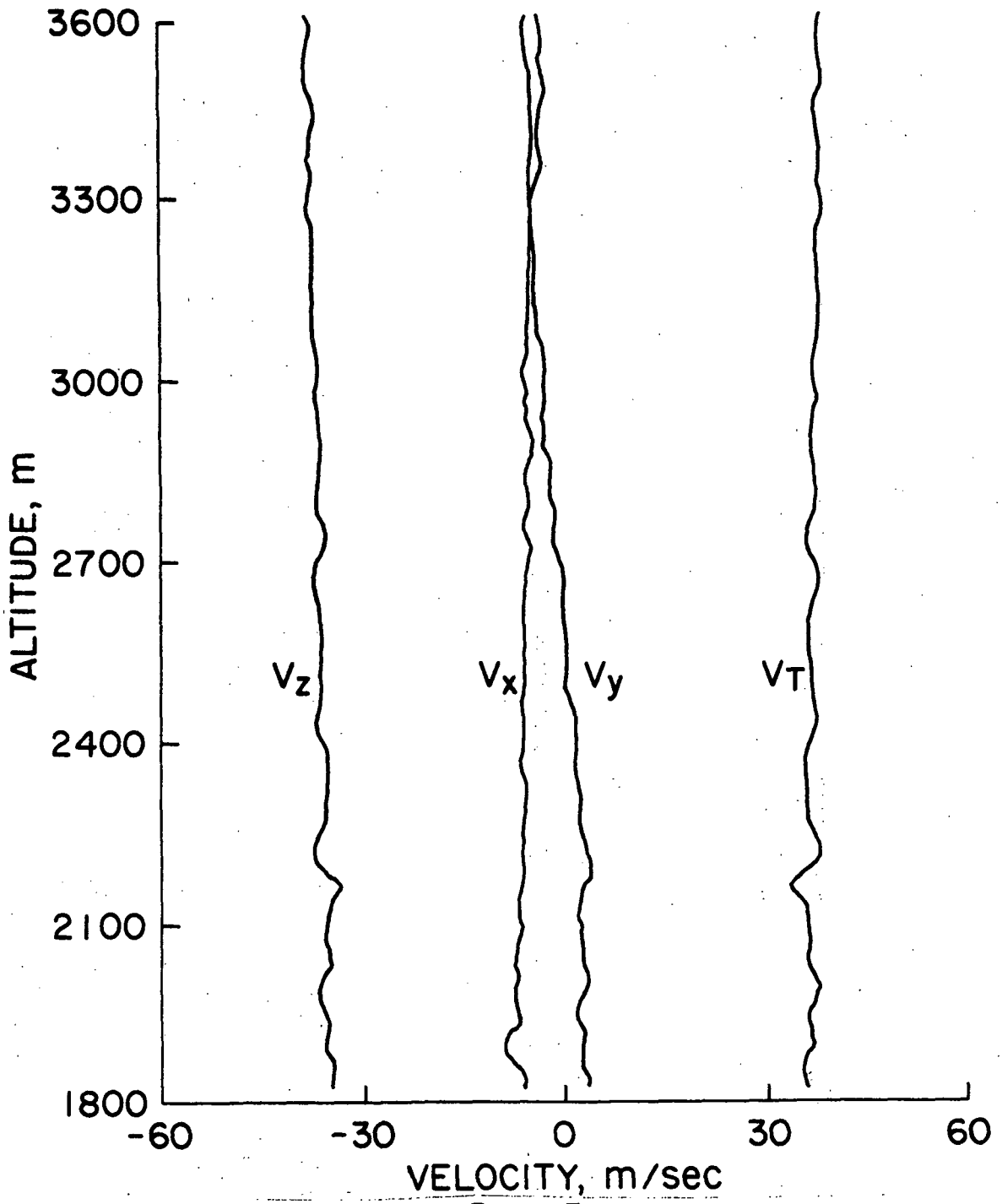

FIGURE 7:
MODEL A3, HORIZONTAL SPIN STABILIZED WITH WIND CORRECTION

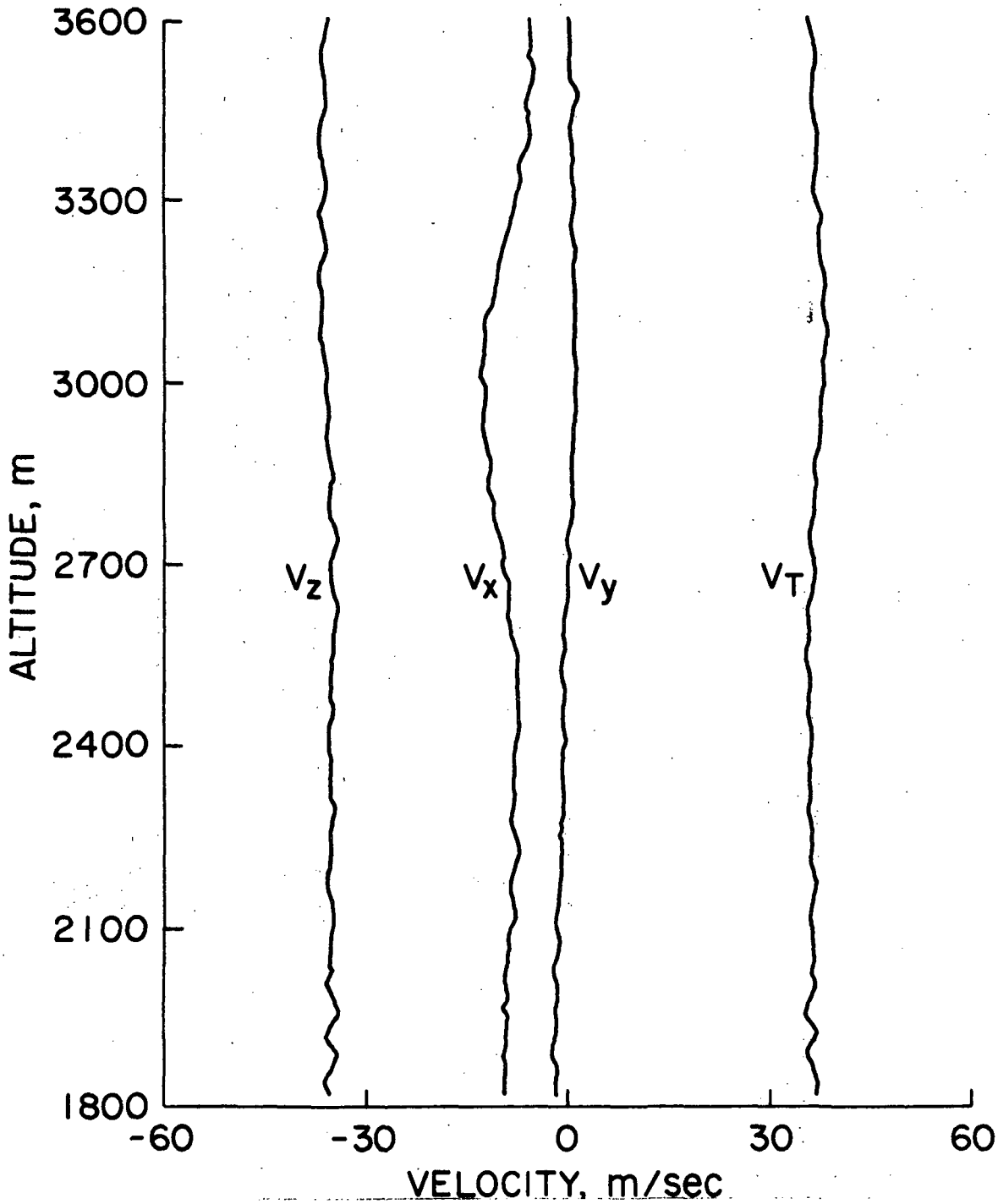

FIGURE 8:

MODEL A4, HORIZONTAL SPIN STABILIZED WITH WIND CORRECTION

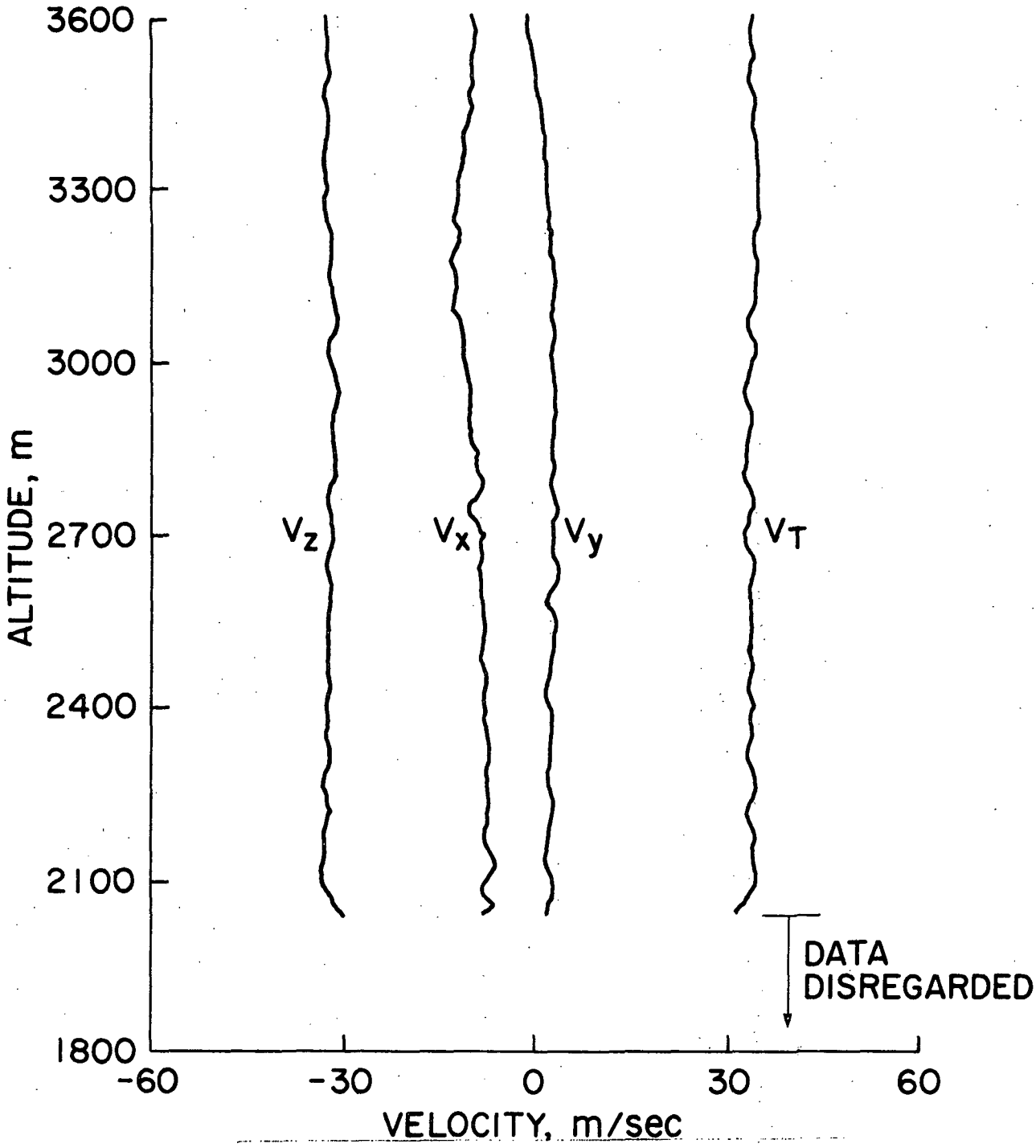

FIGURE 9:
MODEL A5, VERTICAL SPIN STABILIZED
WITH WIND CORRECTION

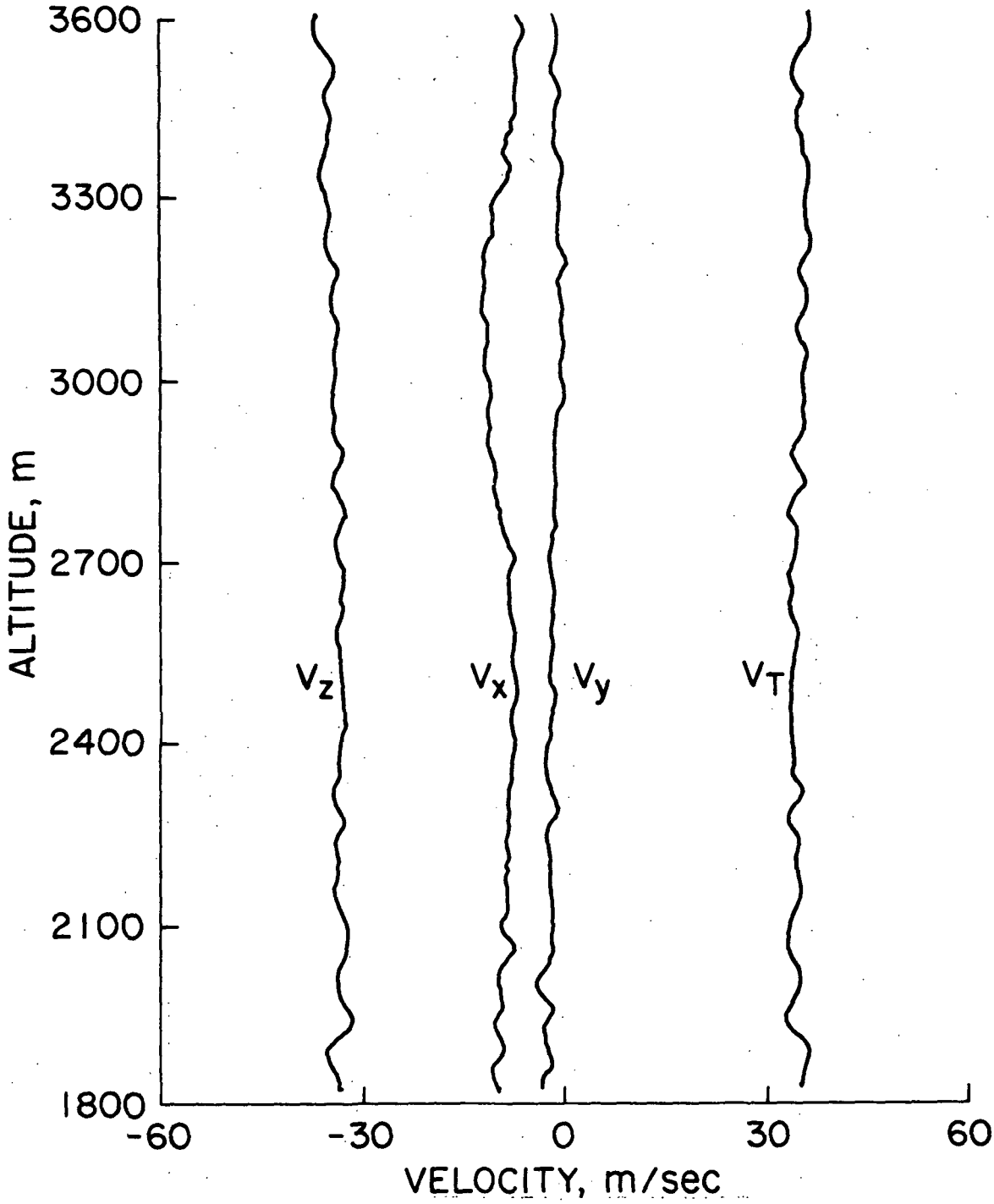

FIGURE 10:

MODEL A6, VERTICAL SPIN STABILIZED WITH WIND CORRECTION

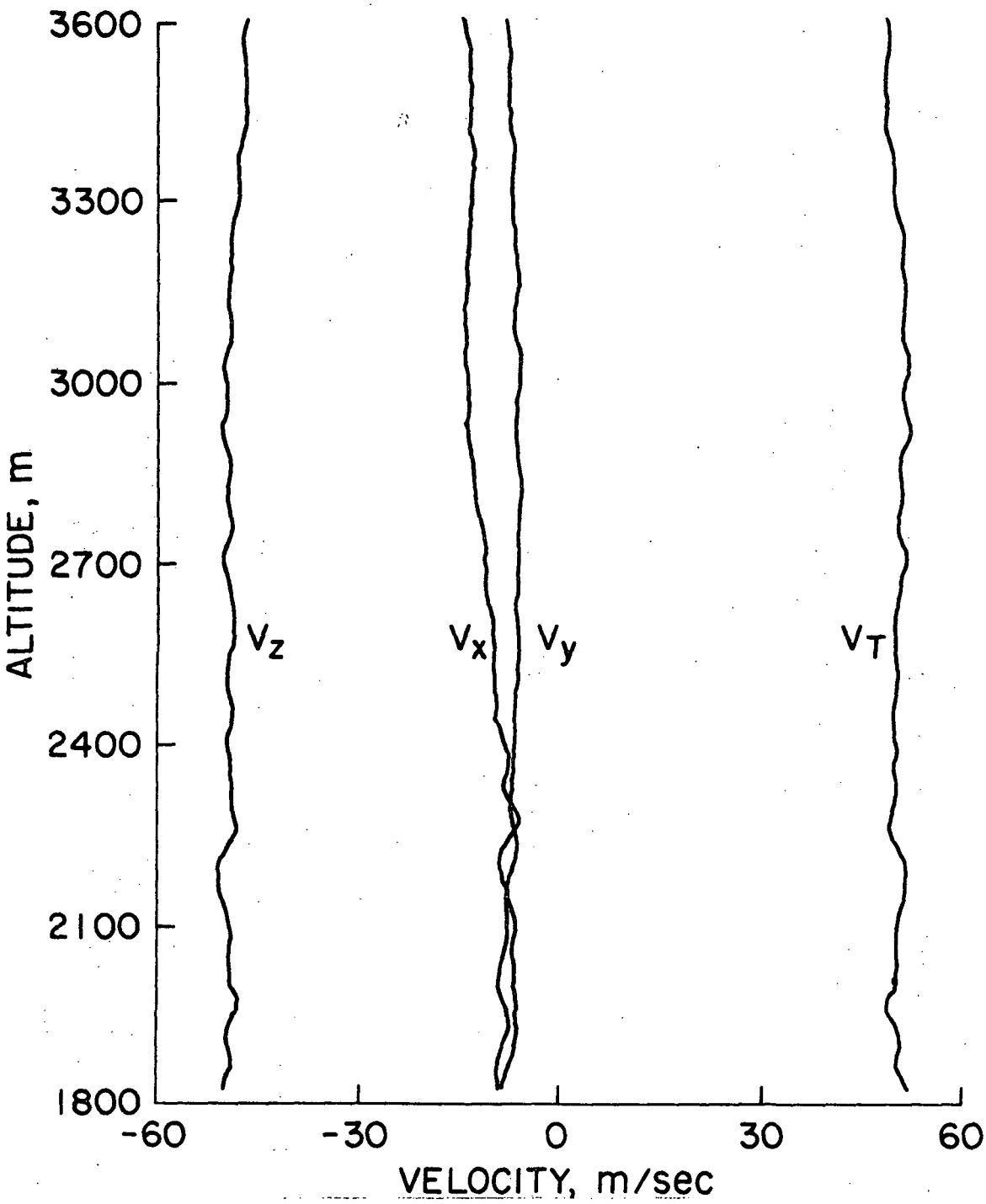

FIGURE 11:

MODEL B1, RANDOM LAUNCHED WITH WIND CORRECTION

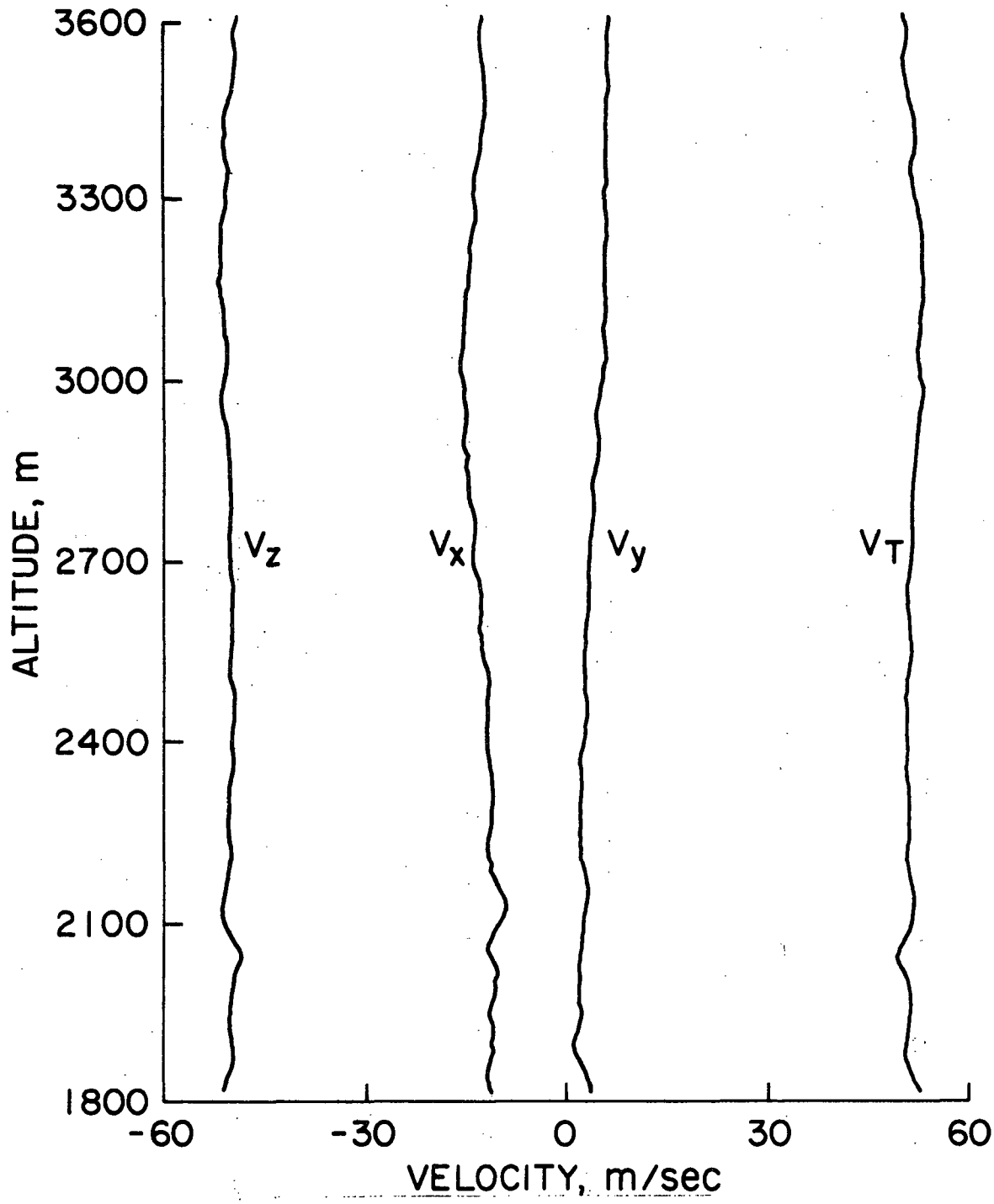

FIGURE 12:
MODEL B2, RANDOM LAUNCHED WITH WIND CORRECTION

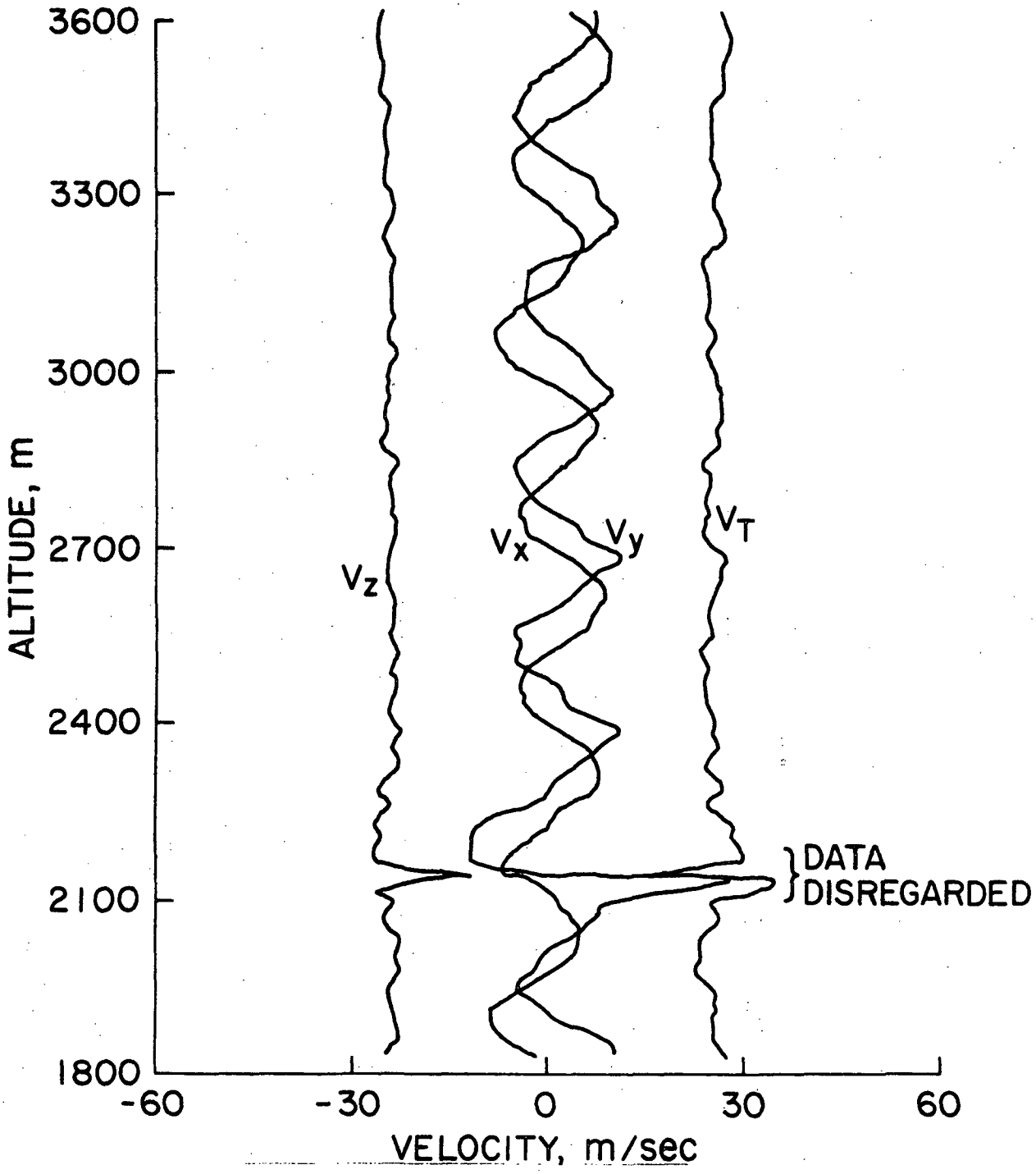

FIGURE 13:

MODEL C1, RANDOM LAUNCHED WITH WIND CORRECTION

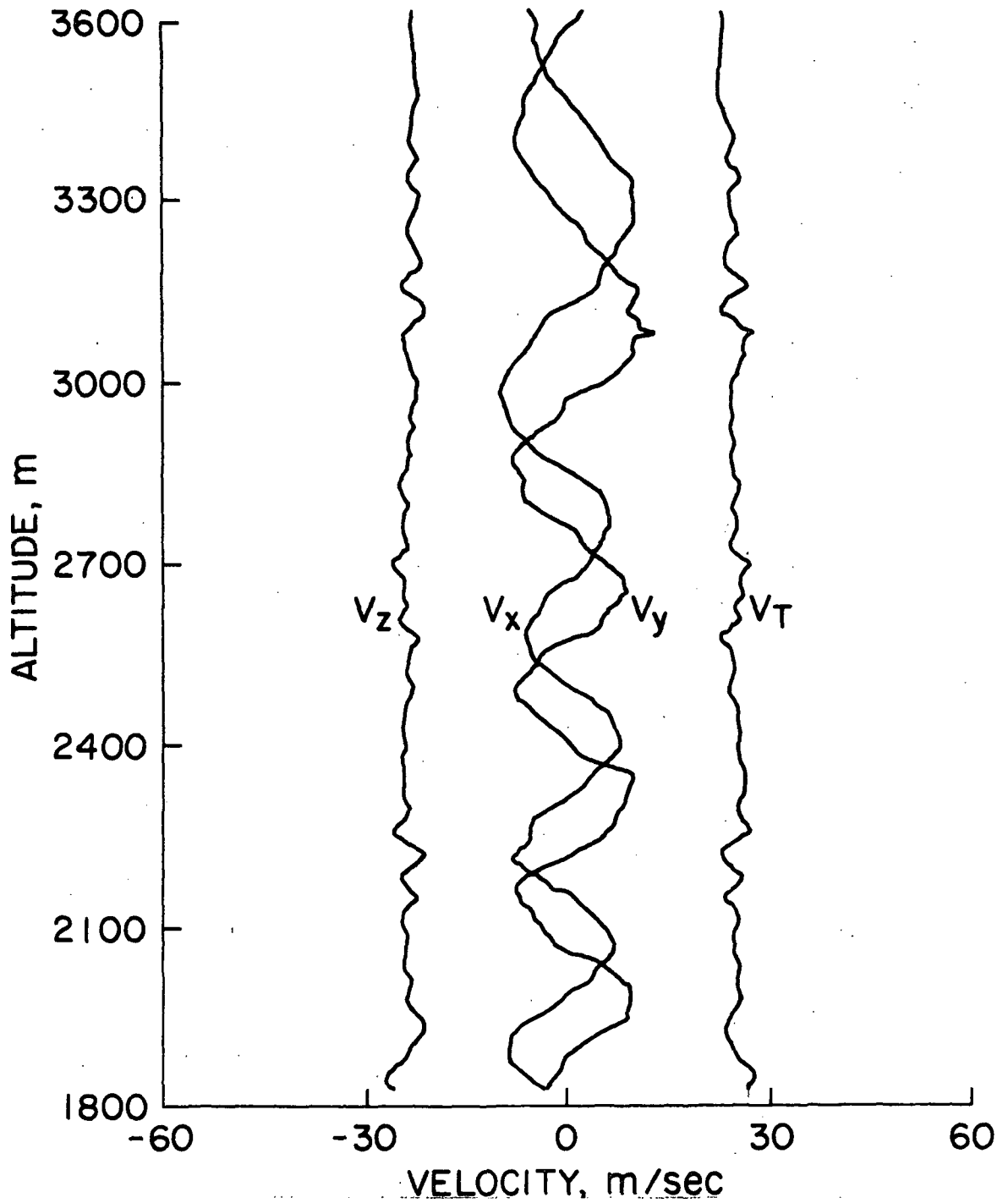

FIGURE 14:

MODEL C2, RANDOM LAUNCHED WITH WIND CORRECTION

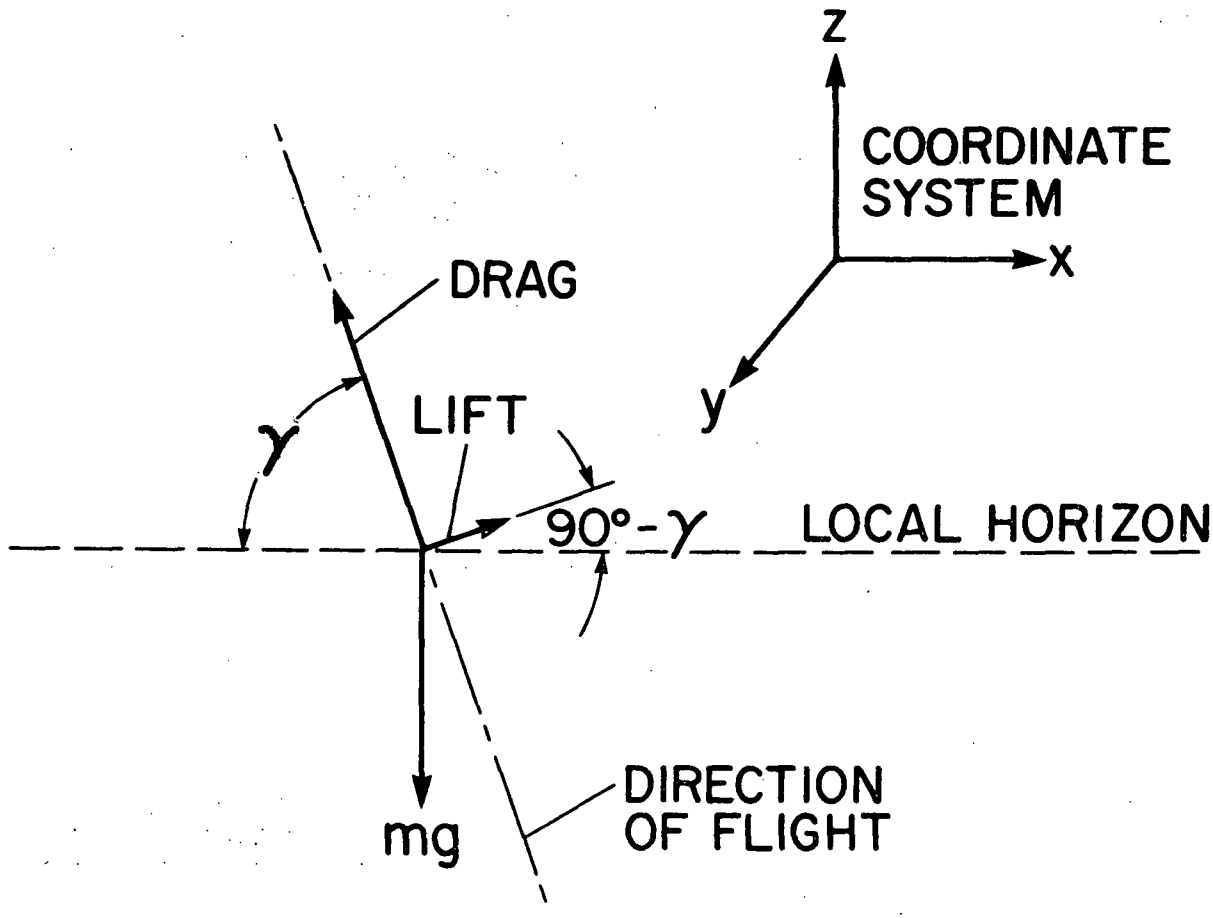

FIGURE 15: FORCES ACTING ON FREE FALLING MODEL

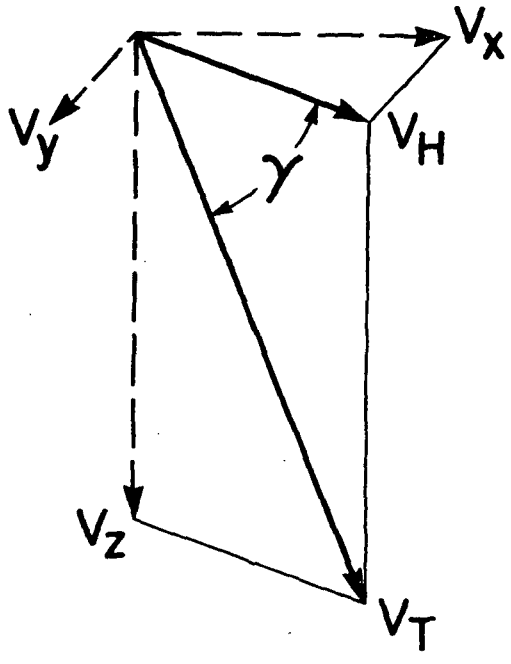

FIGURE 16:

VELOCITY COMPONENTS RESOLVED INTO HORIZONTAL AND TOTAL COMPONENTS

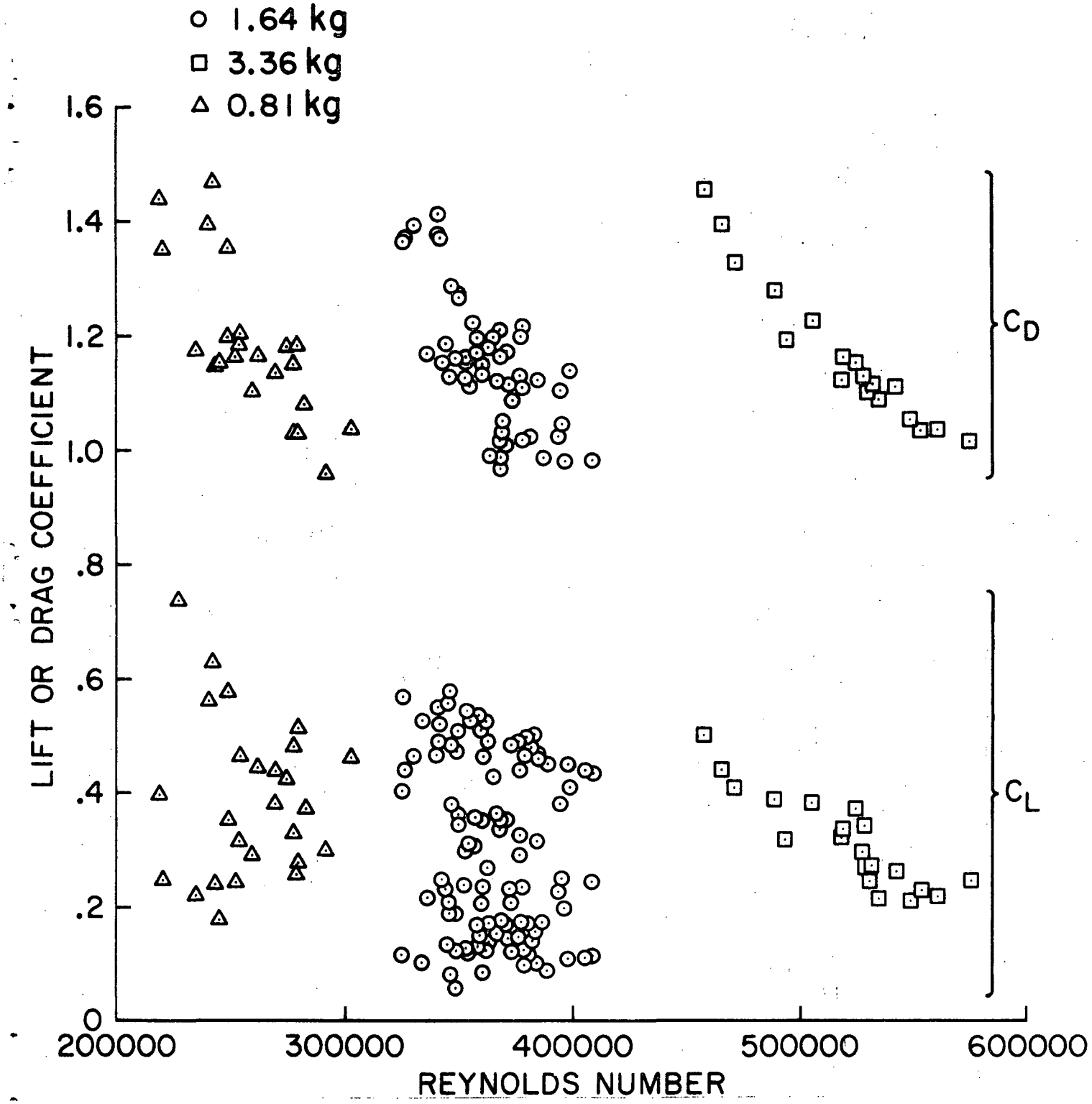

FIGURE 17:

LIFT AND DRAG COEFFICIENT VS REYNOLDS NUMBER

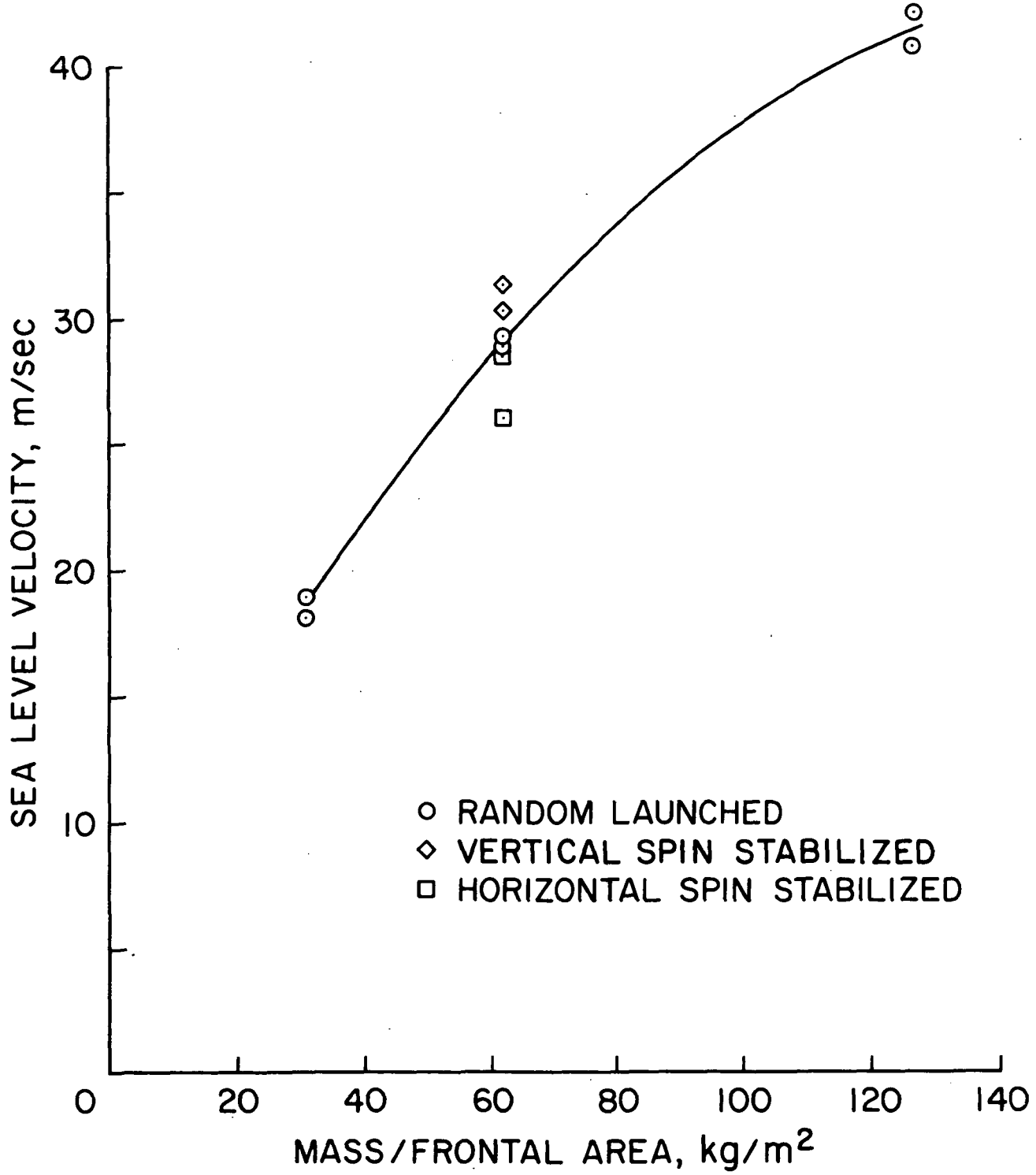

FIGURE 18:

SEA LEVEL VELOCITY VS MASS PER UNIT FRONTAL AREA

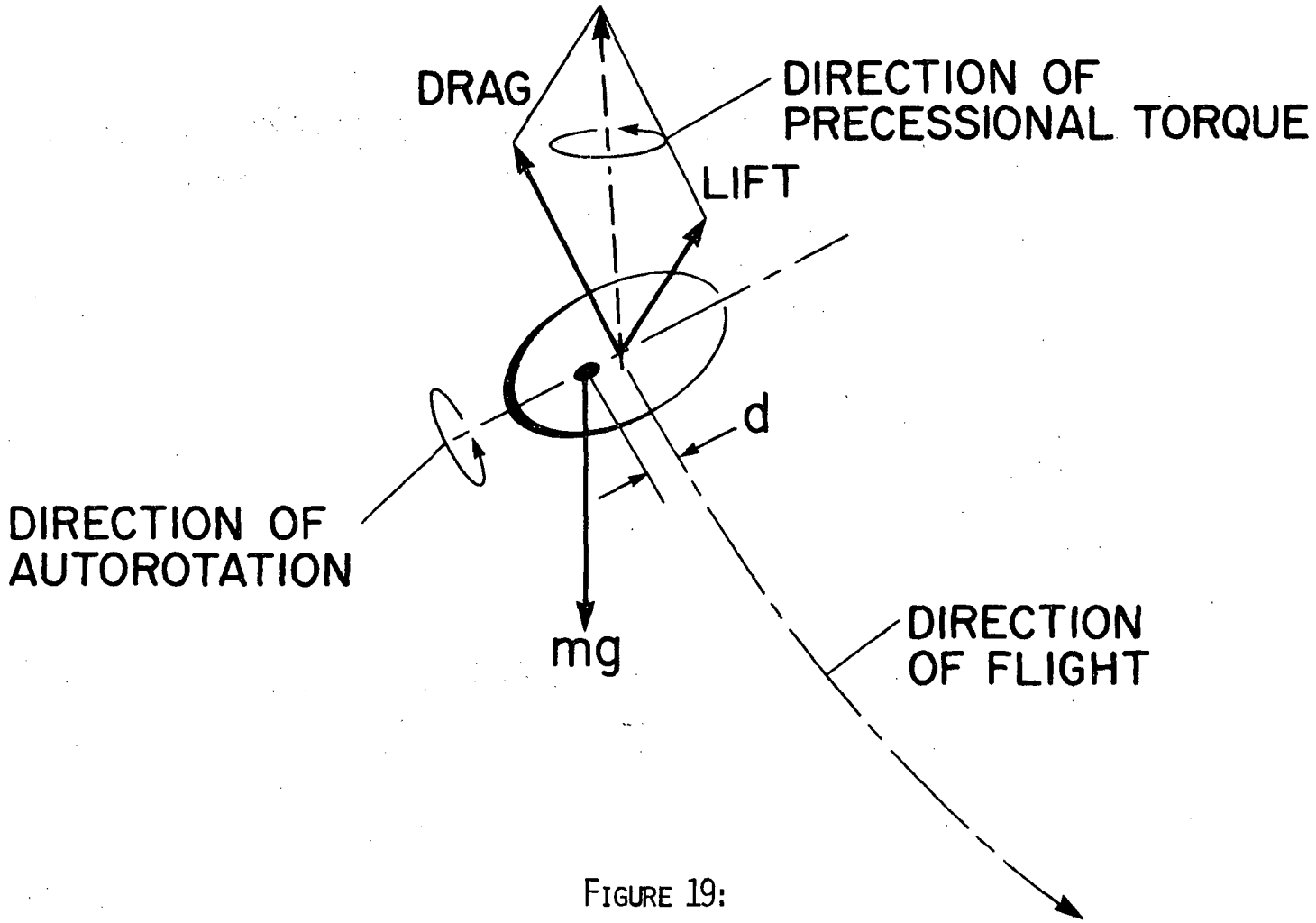

FIGURE 19:

FORCES ON AUTOROTATING DISK
CAUSING SPIRAL FLIGHT